# Supporting Information

**Enhancing Enzyme-like Activities of Prussian Blue Analog Nanocages by Molybdenum Doping: Towards Cytoprotecting and Online Optical Hydrogen Sulfide Monitoring**

Chao Wang, Guoyuan Ren, Binbin Yuan, Wang Zhang, Mingju Lu, Jia Liu, Kai Li, Yuqing Lin*

*Department of Chemistry, Capital Normal University, 105 West Third Ring Road North, Haidian District, Beijing, 100048, China.*

∗Corresponding author: Y. Lin. E-mail address: linyuqing@cnu.edu.cn

## Table of Contents

## EXPERIMENTAL SECTION

**Reagents and Instrumentation.** Potassium hexacyanoferrate(III) ($K_3[Fe(CN)_6]$), nickel nitrate hexahydrate $Ni(NO_3)_2 \cdot 6H_2O$, sodium citrate, ammonium thiomolybdate ($(NH_4)_2MoS_4$), 3,3',5,5'-Tetramethylbenzidine (TMB), 1,2-diaminobenzene (OPD), 2,2′-azino-bis(3-ethylbenzothiazoline-6-sulfonic acid) (ABTS), nicotinamide adenine dinucleotide (NADH), laccase, epinephrine (E), ascorbic acid (AA), dopamine (DA), 3,4-dihydroxyphenylacetic acid (DOPAC), glycine (Gly), glutamate (Glu), glutathione (GSH), cysteine (Cys), histidine (His), uric acid (UA), glucose, sodium sulfide ($Na_2S$), terephthalic acid (TA), 2,7-dichlorodi-hydrofluorescein diacetate (DCFH-DA), dimethyl sulfoxide (DMSO), N,N-dimethylformamide (DMF) and Rosup were all purchased from Sigma (Shanghai, China). Other chemicals with analytical reagent grade were obtained from Beijing Chemical Reagent Company (Beijing, China). The artificial cerebrospinal fluid (aCSF) composed of 126 mM NaCl, 2.4 mM KCl, 1.1 mM $CaCl_2$, 0.85 mM $MgCl_2$, 27.5 mM $NaHCO_3$, 0.5 mM $Na_2SO_4$, 0.5 mM $KH_2PO_4$ with pH to be 7.4 was used as solution for online measurement experiments.

The SEM (Scanning Electron Microscopy) images were conducted using a Hitachi SU8010 scanning electron microscope; TEM (transmission electron microscope) images, HRTEM (high-resolution TEM), elemental mapping and EDS (energy-dispersive spectroscopy) analyses were obtained on a JEM-2100F transmission electron microscope operated at 200 kV; The nitrogen adsorption and the Barrett-Joyner-Halenda (BJH) model was used to calculated specific surface area;

FT-IR (flourier transform infrared) spectra were accomplished by Bruker Equinox55 spectrophotometer; A Bruker D8 advance powder diffractometer with Cu Kα radiation was used to carry out XRD (X-ray powder diffraction) spectra; An ESCA Lab 250 X-ray photoelectron spectrometer using a monochromatic Al Kα radiation excitation source was used to measure XPS (X-ray photoelectron spectra); The fluorescence spectra and UV-Vis (ultraviolet-visible) absorption spectra were gained by Hitachi FL4500 fluorescence spectrophotometer and Shimadzu UV-2550 UV-Vis spectrophotometer respectively; The electrochemical measurements were recorded by a CHI1000C (Chenhua) potentiostat. The glass carbon electrodes as work electrode, Ag/AgCl electrode as reference electrode, Pt electrode as the compared electrode; The fluorescence microscope (IX73, Olympus, USA) was used in taking fluorescence (under 365 nm laser excitation) and bright-field images of cells. The IX73 microscope was also used in $H_2S$ online manner. All bright field images inside the capillary (Φ250 μm) were captured with time interval of 5 s, and followed by transforming to real-time light intensity profile by CellSens Dimension 2.1 software at the same time.

**Synthesis of Prussian Blue Analog Nanocubes.** Prussian blue analog based nanocubes (PBA) was synthesized by water bath assisted method. Typically, sodium citrate (0.9 mmol) and $Ni(NO_3)_2 \cdot 6H_2O$ (0.6 mmol) were dissolved in DI water (20 mL) as solution A, while $K_3[Fe(CN)_6]$ (0.4 mmol) was dissolved in DI water (10 mL) as solution B. Then, solution A and B was quickly mixed at room temperature. After heating the beaker at 40 °C water bath for 24 h, the precipitate was collected by centrifugation, and washed with DI water twice. Finally, the powder (PBA) was

obtained after dried at 60 °C overnight.

**Analysis of Enzyme-like Activity of Nanocages.** Analysis of peroxidase-like activity: The reaction solutions (pH 7.0) containing TMB (1 mL, 2 mM), $H_2O_2$ (1 mL, 10 mM), and Nanocages (1 mL, 100 μg/mL) were mixed and UV-Vis absorption spectra were recorded. OPD, ABTS and NADH systems were performed the same as TMB system.

Analysis of catalase-like activity: The reaction solutions (pH 7.0) containing TA (1 mL, 0.5 mM), $H_2O_2$ (1 mL, 50 mM), and Nanocages (1 mL, 0, 10, 25, 50 and 100 μg/mL) were mixed at room temperature and pH 7.0. Besides, another group (concentration of nanocages: 0, 10, 25, 50 and 100 μg/mL) was incubated under 365 nm UV light for 20 min first. Then, the fluorescence spectra of each reaction solutions were measured by fluorescence spectrophotometer.

Analysis of laccase-like activity: The reaction solutions (pH 7.0) containing DA (1mL, 100 μg/mL) and Nanocages (1mL, 100 μg/mL). The brown color oxidized products were investigated by scanning the UV-Vis absorbance on spectrophotometer at 450 nm.

**Kinetic Analysis of Nanocages in Laccase-like activity.** The steady-state kinetic analysis of laccase-like activity of Nanocages were carried out in reaction mixture solutions (pH 7.0) with volume of 2.0 mL containing DA as substrate (1 mL, difference concentrations) and Nanocages (1 mL, 100 μg $mL^{-1}$). Then, the resulting solutions were used for absorbance measurement at 450 nm. The Michaelis-Menten constant was calculated by applying a Lineweaver-Burk plot ((1/V = $K_m/V_{max}$ (1/[S] +

$1/K_m$), where V is the initial velocity, $V_{max}$ is the maximal reaction velocity, [S] is the substrate concentration, and $K_m$ is the Michaelis-Menten constant).

**Cell Culture.** Hela cells were cultured under 5% $CO_2$ at 37 °C in air with normal growth medium consisting of high-glucose DMEM. The cell growth media contained 10% FBS, 100 mg/mL streptomycin and 100 U/mL penicillin. The media was renewed every 48 h, and the cells were digested by trypsin and resuspended in fresh medium before plating.

**Cytotoxicity Assays.** Hela cells were seeded in 96-well plates, and incubated for 24 h before interacting with materials. Then, Nanocages were added to the cell culture medium and incubated for 24 h and 48h, respectively. Finally, MTT solution was added to each well in plates and recorded by standard MTT assay.

**In Vivo Microdialysis and $H_2S$ Monitoring In Brains of Living Rats.** Adult male Sprague-Dawley rats (SD rats, weighing 300 ± 50 g) were obtained from Vital River Laboratory Animal Technology Co., Ltd. (Beijing, China). The rats were housed individually with a 12:12 h light/dark schedule. Briefly, guide tubes were inserted into rat brain under anesthetized by chloral hydrate (350 mg/kg i.p.). For the $Na_2S$ intraperitoneal injection model, the microdialysis probe (4 mm in length; Bioanalytical Systems Inc. (BAS), BAS Carnegie Medicine) was implanted into the brain hippocampal region (AP=4.5 mm, L=4.2 mm from bregma, V=2.5 mm from the surface of the skull) according to standard stereotaxic procedures. Before microdialysis and online optical measurements, the rats were allowed to recover for 24 h. The microdialysis sampling was perfused with aCSF at a flow rate of 2 μL/min

to monitor the cerebral $H_2S$ levels with the microdialysates flowing into the OODP continuously. The 0.9 % saline and $Na_2S$ solution (40.8 mg/kg) were injected into the same rat by intraperitoneal injection.

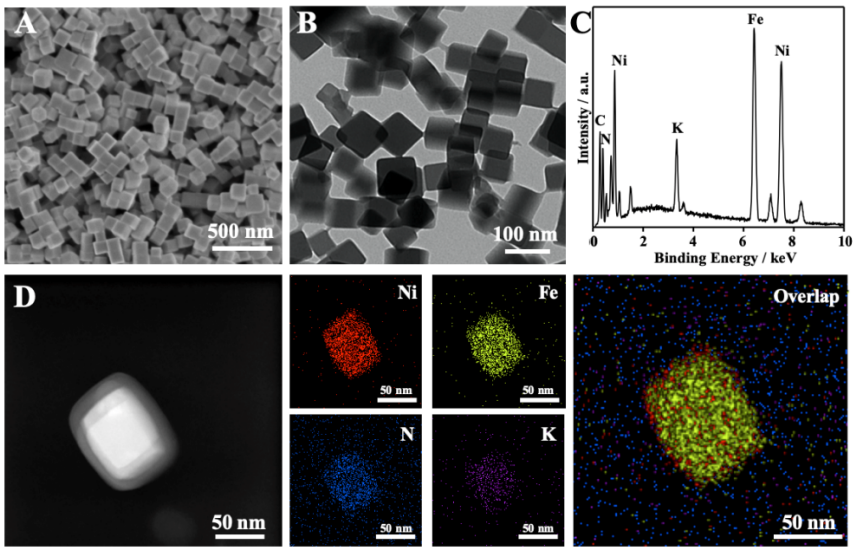


**Figure S1.** SEM image (A); TEM image (B); EDS spectrum (C) and elements mapping images (D) of PBA nanocubes (PBA).

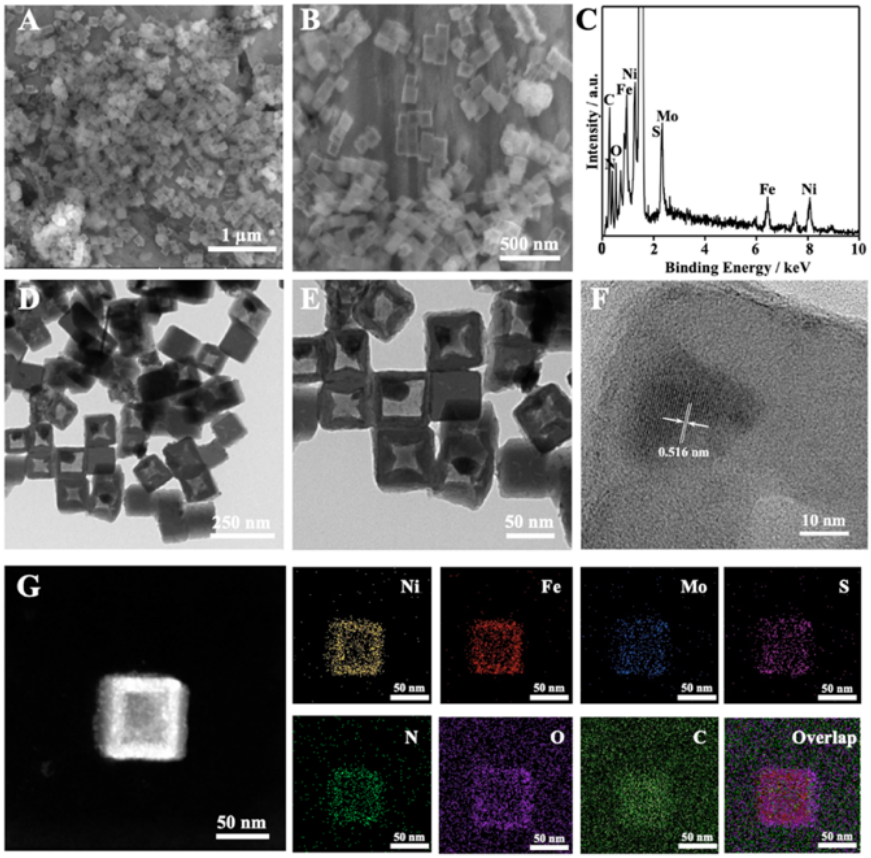


**Figure S2.** Typical SEM images (A, B); EDS spectrum (C); TEM images (D, E); HRTEM image (F) and elements mapping images (G) of Nanocages.

The HRTEM images (Figure S2F) show lattice spacing of 0.516 nm, which just indicated a typical (200) plane of $KNi[Fe(CN)_6]$ crystalline types and is in consistent with XRD results.

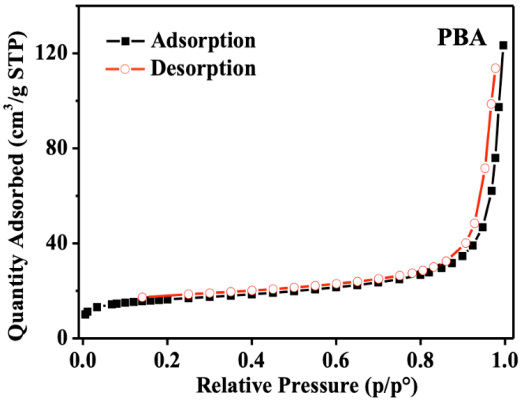


**Figure S3.** The $N_2$ adsorption-desorption isotherms of the PBA to measure the specific surface area.

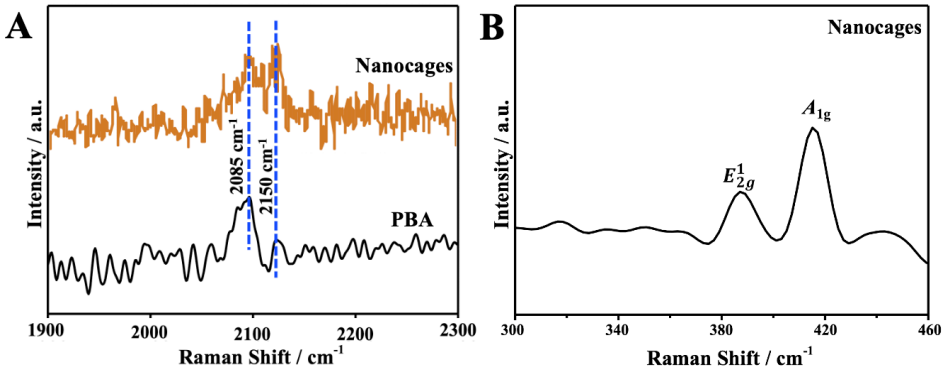


**Figure S4.** (A) Raman spectra of PBA and Nanocages. (B) Raman spectrum of Nanocages in lower Raman shift range.

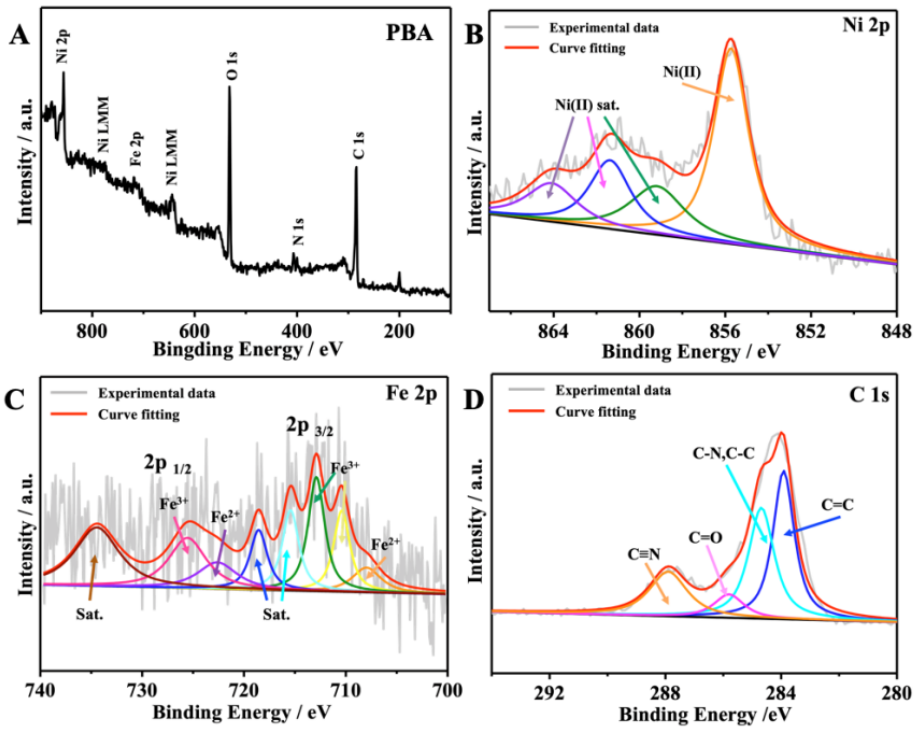


**Figure S5.** (A) XPS survey spectra of PBA. High-resolution XPS spectra of (B) Ni 2p, (C) Fe 2p and (D) C 1s of PBA.

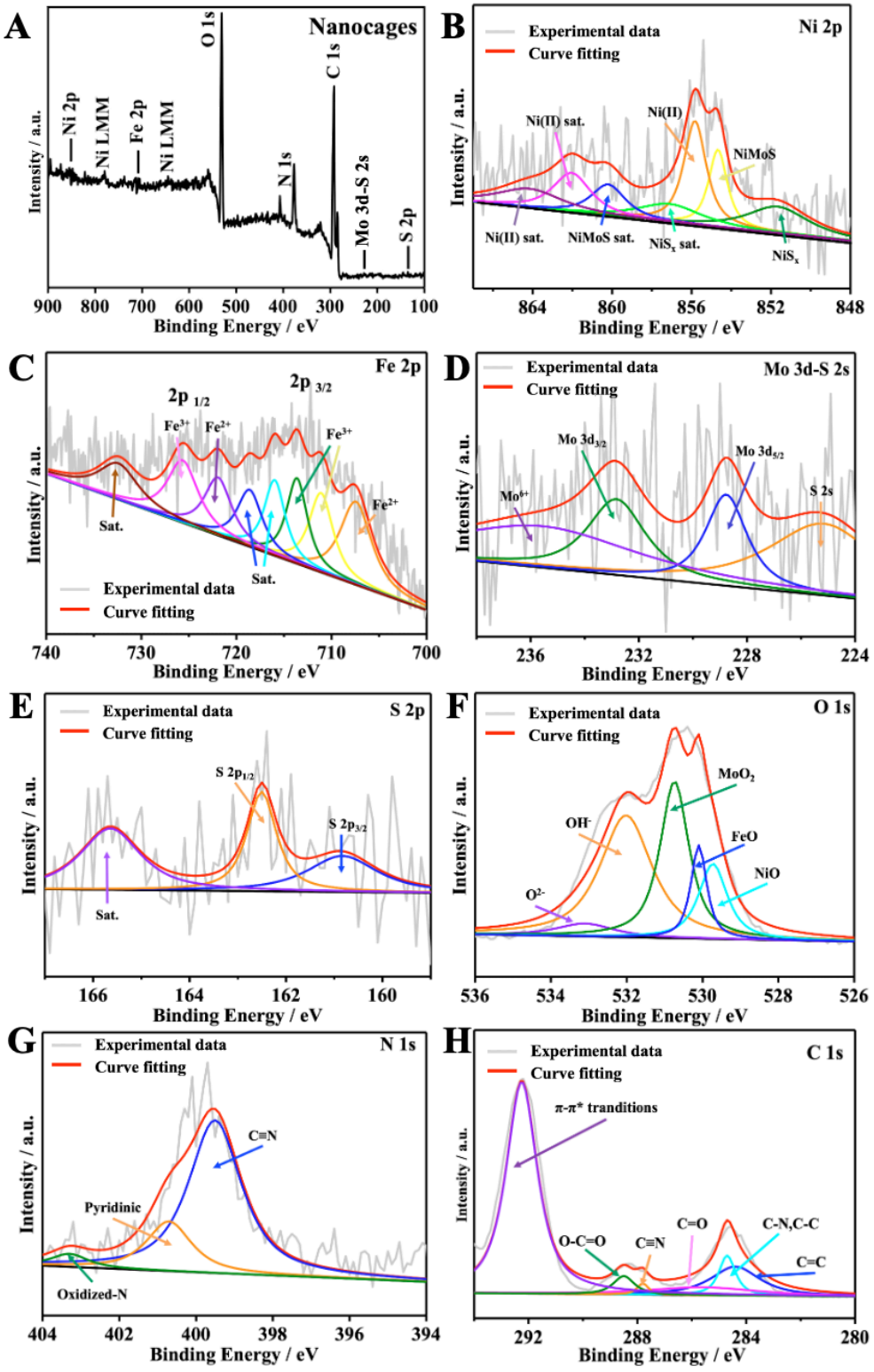


**Figure S6.** (A) XPS survey spectra of Nanocages, and (B-H) high-resolution XPS spectra of Ni 2p, Fe 2p, Mo 3d-S 2s, S 2p, N 1s, O 1s and C 1s.

**XPS Analysis of PBA and Nanocages.**

To thorough investigate the surface chemical compositions and valence states changes of each metal, XPS spectra were performed on PBA first (Figure S5). The XPS spectra of Ni 2p (Figure S5B) and Fe 2p (Figure S5C) show Ni(II) species (855.7 eV),[S1] $Fe^{3+}$ (711.4 eV, 714.6 eV, 725.6 eV, 79%) and $Fe^{2+}$ (708.4 eV, 721.9 eV, 21%) were the mainly form of metals in PBA. The C1s spectrum (Figure S5D) shown the C-N bond (285.1 eV) and C≡N bond (288.3 eV) in $KNi[Fe(CN)_6]$, as well as C=C bond (284.6 eV), C-C bond (285.1 eV) and C=O bond (287.1 eV) from sodium citrate.

For Nanocages, the synthesis processes were accomplished by two steps, a sulfide etching follows by molybdenum polysulfide nanoparticles depositing. The signals of Ni, Fe, Mo, S, N, O and C were detected in the overall XPS spectrum of the Nanocages (Figure S6A). Especially, the S peak existed, indicating that the ion exchanged between $[Fe(CN)_6]^{3-}$ and $S^{2-}$ ions happened and lead to the formation of hollow-centered Nanocages. The composition of Ni (Figure S6B) in 2+ states (855.9 eV),[S2] Fe (Figure S6C) in 61% of 3+ states (711.1 eV, 713.7 eV, 726.1 eV) and 39% of 2+ states (708.4 eV, 722.8 eV) were calculated from the spectra respectively.[S3] It was found that a small quantity of NiMoS (855.1 eV) and $NiS_x$ (851.9 eV) existed from Ni 2p spectra,[S4] which may belong to the $S^{2-}$ ions replacing $[Fe(CN)_6]^{3-}$ partially during ion exchange. On the other hand, under solvothermal conditions, a parts of Fe(III) in $[Fe(CN)_6]^{3-}$ were reduced into Fe(II), and finally released into the solution.[S5] These oxidation states of the transition metals are related to the number of valence electrons.

The Mo 3d-S 2s spectrum (Figure S6D) suggested that Mo (IV) (233.1 eV, 228.8 eV) and (235.7 eV) of Mo element existed together in the structure, while appearing of Mo(VI) due to partial oxidation of Mo(IV).[S6] The peaks located at 225.5 eV was corresponded to S 2s, indicating the evidence of Mo-S bond existence. Meanwhile, binding energy at 160.8 eV in the S 2p spectrum (Figure S6E) can be corresponded to low valence state of sulfur ions and another peak (162.5 eV) to metal-sulfur bonding, while a peak at 165.5eV was attributed to one shakeup satellite peak.[S7] Constructed Mo 3d spectrum and S 2p spectrum together, the results suggested that a few $MoS_x$, NiMoS and $NiS_x$ were appeared in the products and the etching and depositing process accomplished successfully.

Otherwise, the O 1s spectrum (Figure S6F) suggested that only a few metal oxide, such as NiO (529.7 eV), FeO (530.1 eV) and $MoO_2$ (530.7 eV), also coexisted in Nanocages. The binding energy loading at 533.1 eV and 532.0 eV were attributed to oxygen ion in low coordination at the surface and oxygen in $OH^-$ group, respectively. Those existed species might be attituded to solve thermal process. In the XRD pattern of Nanocages, no peaks of $MoS_x$, NiMoS, $NiS_x$ and few metal oxides were observed, although those were detected in XPS spectra, which indicated that its amount might be negligibly low. In N 1s spectrum (Figure S6G), the binding energy loaded at 399.5 eV and 400.9 eV were corresponded to C≡N bond and pyridinic-N. The peaks of oxidized-N (402.9 eV) in N 1s spectrum (Figure S6G), as well as the new peaks of π-π* transition (292.3 eV) and O-C=O (288.2 eV) in C 1s spectra (Figure S6H) indicated that the CN group in the PBA precursors were converted into N-doped

carbon in the Nanocages.[S8] The peaks of C≡N bond and C=C bond downshifted to 287.9 eV and 284.1 eV in C 1s spectrum of Nanocages. As previously reported, this downshift of binding energy indicates appropriate modulation toward electronic structure and possibly suggests the increase of electron number, which is closely related to enhanced catalytic property.[S9] By appropriating modulation toward chemical composition and electronic structure, the increasing electron number was probably suggested, which may further enhance catalytic performance.[S10]

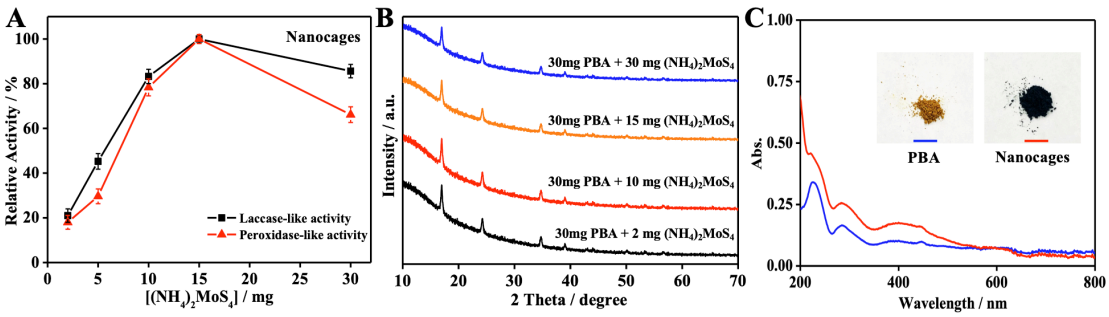


**Figure S7.** (A) Comparison of as-synthesized nanocages at different mass of $(NH_4)_2MoS_4$ (2, 5, 10, 15, 30 mg) to oxidize DA (100 μg/mL) for laccase-like catalytic efficiency the absorbance at 450 nm, and TMB (2 mM) and $H_2O_2$ (10 mM) for peroxidase-like catalytic efficiency the absorbance at 650 nm. (B) XRD patterns of the as-synthesized products of Nanocages at different doses of $(NH_4)_2MoS_4$. (C) UV-Vis absorption spectra and photography of PBA and Nanocages.

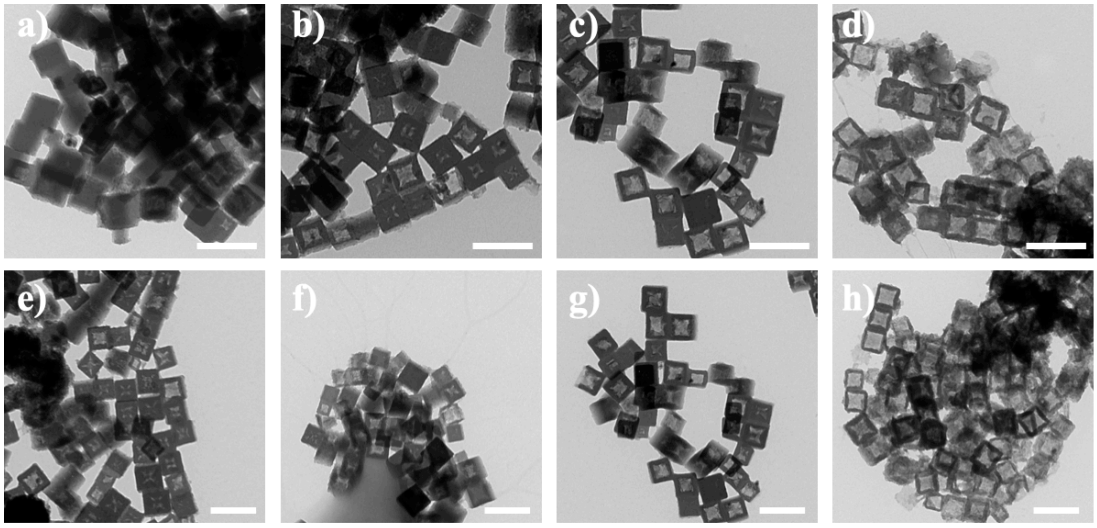


**Figure S8.** TEM images of the as-synthesized products of Nanocages at different mass of $(NH_4)_2MoS_4$: 5 mg (a, e), 10 mg (b, f), 15 mg (c, g) and 30 mg (d, h). All scale bar presents 200 nm.

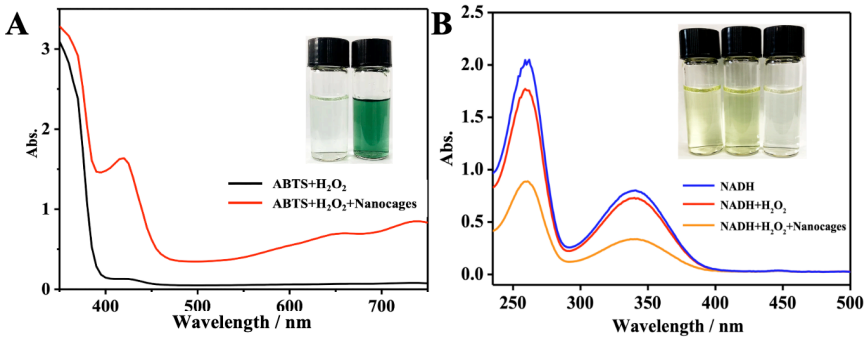


**Figure S9.** Absorption spectra of ABTS (A) and NADH (B) catalyzed oxidation by Nanocages with $H_2O_2$.

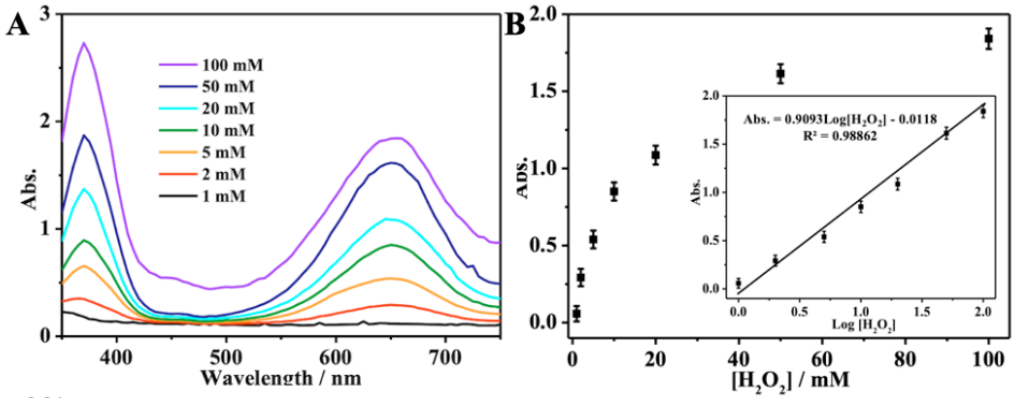


**Figure S10.** $H_2O_2$ colorimetric sensing based on Nanocages. (A) Absorption spectra of TMB with different $H_2O_2$ concentrations. (B) A dose-response curve for $H_2O_2$ detection at 650 nm. Inset shows the linear relationship between absorbance values with the log[$H_2O_2$] in the range from 1 to 100 mM.

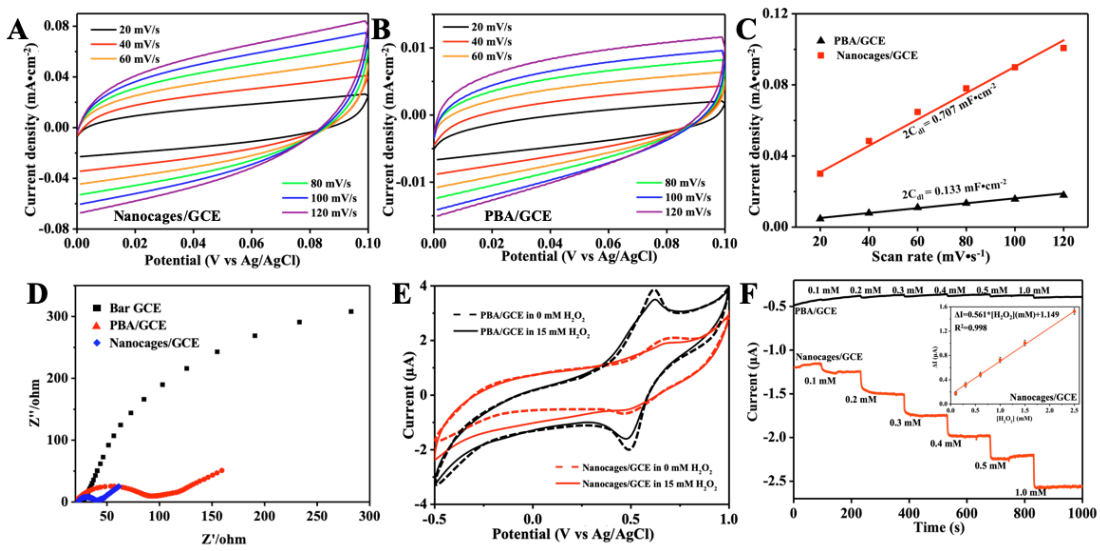


**Figure S11.** Cyclic voltammograms for Nanocages/GCE (A) and PBA/GCE (B). (C) ECSA evaluation of Nanocages/GCE and PBA/GCE. (D) EIS at 1.125V versus Ag/AgCl of Nanocages/GCE, PBA/GCE and bar GCE. (E) CVs of the Nanocages/GCE (red line) and PBA/GCE (black line) in phosphate buffer solution in the presence (solid line) and absence (dash line) of 5 mM $H_2O_2$. (F) Amperometric response of the Nanocages/GCE (red line) and PBA/GCE (black line) with an increasing concentration of $H_2O_2$ at a potential of -0.3 V (as opposed to Ag/AgCl). Inset shows the linear relationship between response current values with the concentrations of $H_2O_2$ in the range from 0.1 to 2.5 mM. Error bars represent the SD of replicates measurements with n = 3.

In order to further evaluated the amount of catalytic active sites, electrochemical active surface area (ECSA) measurements were carried out, which was in proportion to electrochemical double-layer capacitance ($C_{dl}$).[S11, S12] Therefore, $C_{dl}$ was calculated by measuring a cyclic voltammetry (CV) curve in an appropriate potential range by

different sweep speeds, in which no significant Faraday process occurred. (Figure S11 A-C). Obviously, Nanocages/GCE showed a much larger 2Cdl of 0.707 mF $cm^{-2}$ than PBA nanocubes/GCE (0.133 mF $cm^{-2}$, PBA/GCE), indicating that the optimal mimicking catalytic performance of Nanocages might be related to the largest ECSA. To further study the catalysis difference between Nanocages and PBA/GCE, electrochemical impedance spectroscopy (EIS) was carried out. As shown in Figure S11D, Nanocages/GCE had a smaller diameter of semicircle than those of PBA/GCE and bar GCE, implying Nanocages exhibited a smaller charge transfer resistance and much faster electron transfer process during electrochemical reaction.[S13] To investigate the reduction process of $H_2O_2$ on the electrode surface, the CV curve of Nanocages/GCE in 15 mM $H_2O_2$ solution revealed a reduction response at -0.3 V, but no response were observed when using PBA/GCE (Figure S11E). Amperometric results on the Nanocages/GCE show that a better response to $H_2O_2$ can be clearly observed, while the PBA/GCE even shown a baseline response (Figure S11F).

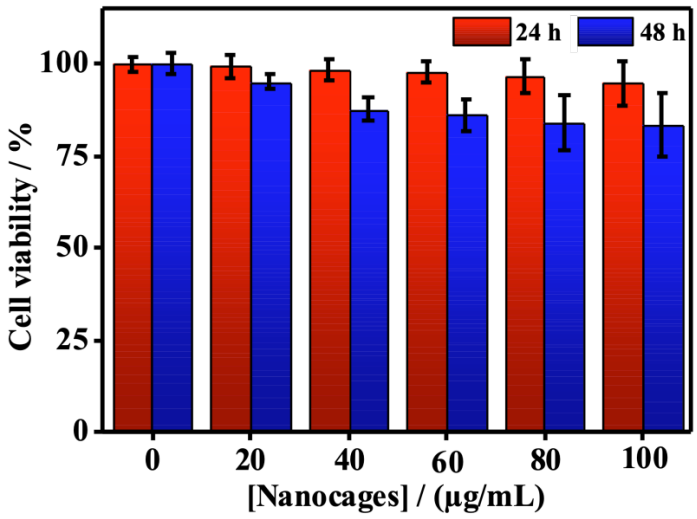


**Figure S12.** Cell viability of Nanocages in Hela cells within 24 and 48 h by MTT assay.

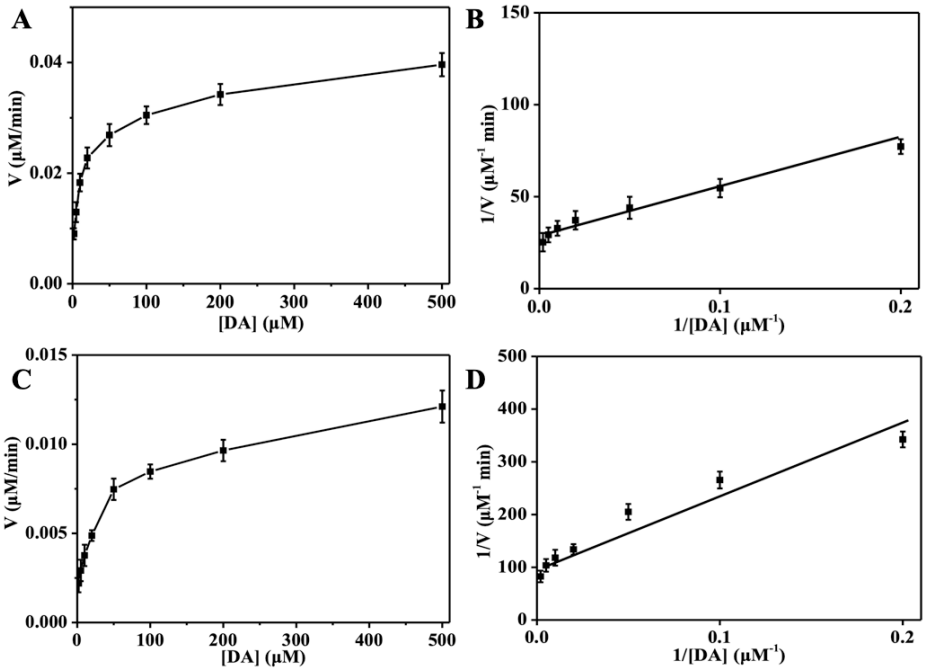


**Figure S13.** Steady-state kinetic assay of laccase-like activity of Nanocages (A, B) and nature laccase (C, D). The concentrations of Nanocages (A) and nature laccase (C) were 100μg/mL and DA concentrations were varied (2, 5, 10, 20, 50, 100, 200 and 500 μM). Double-reciprocal plots of activity of Nanocages (B) and nature laccase (D) of the substrate for DA. Error bars represent the SD of replicates measurements with n = 3.

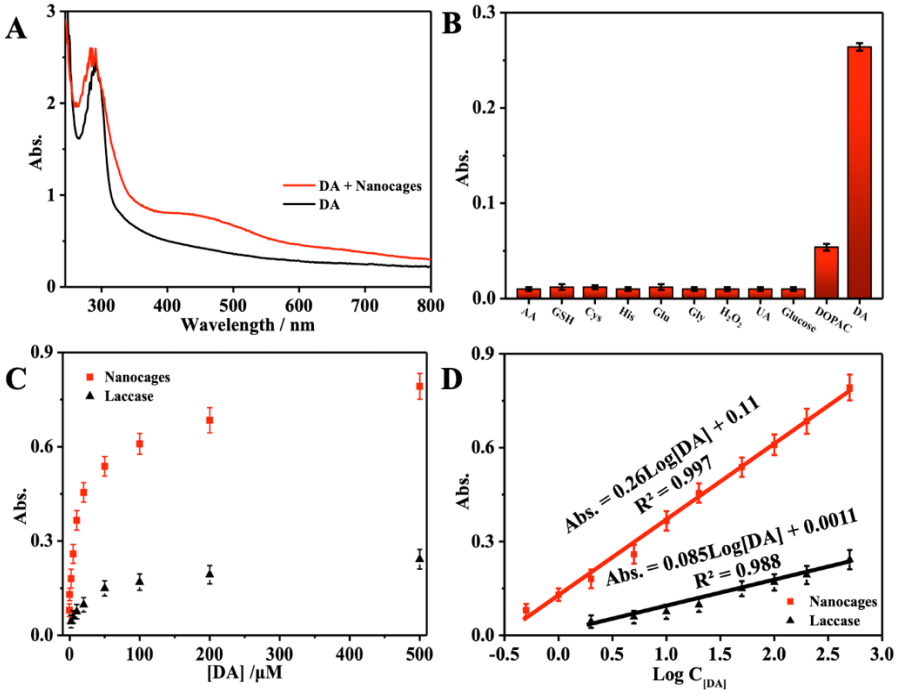


**Figure S14.** (A) UV-Vis spectra of DA and its oxidation product by the Nanocages. (B) Selectivity investigations of Nanocages for sensing DA. (C) The relationships between the absorbance at 450 nm and the concentration of DA (in aCSF) in the presence of Nanocages and laccase. (D)The linear relationship of absorbance to DA. Error bars represent the SD of replicates measurements with n = 3.

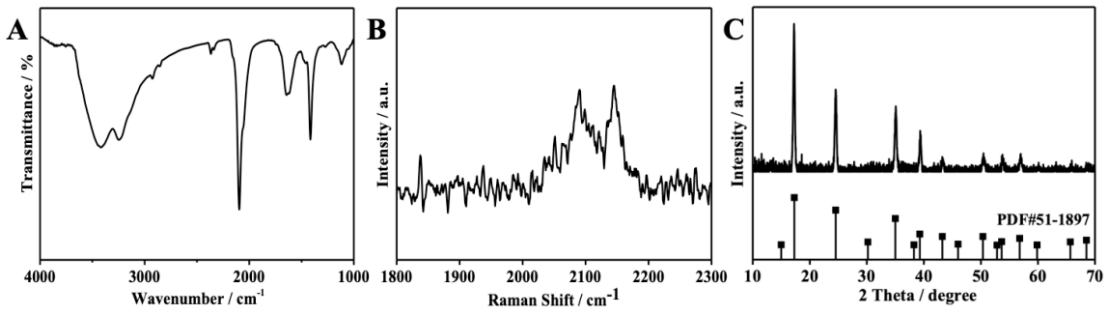


**Figure S15.** The (A) FT-IR spectrum, (B) Raman spectrum and (C) XRD pattern of Nanocages after reacting with DA.

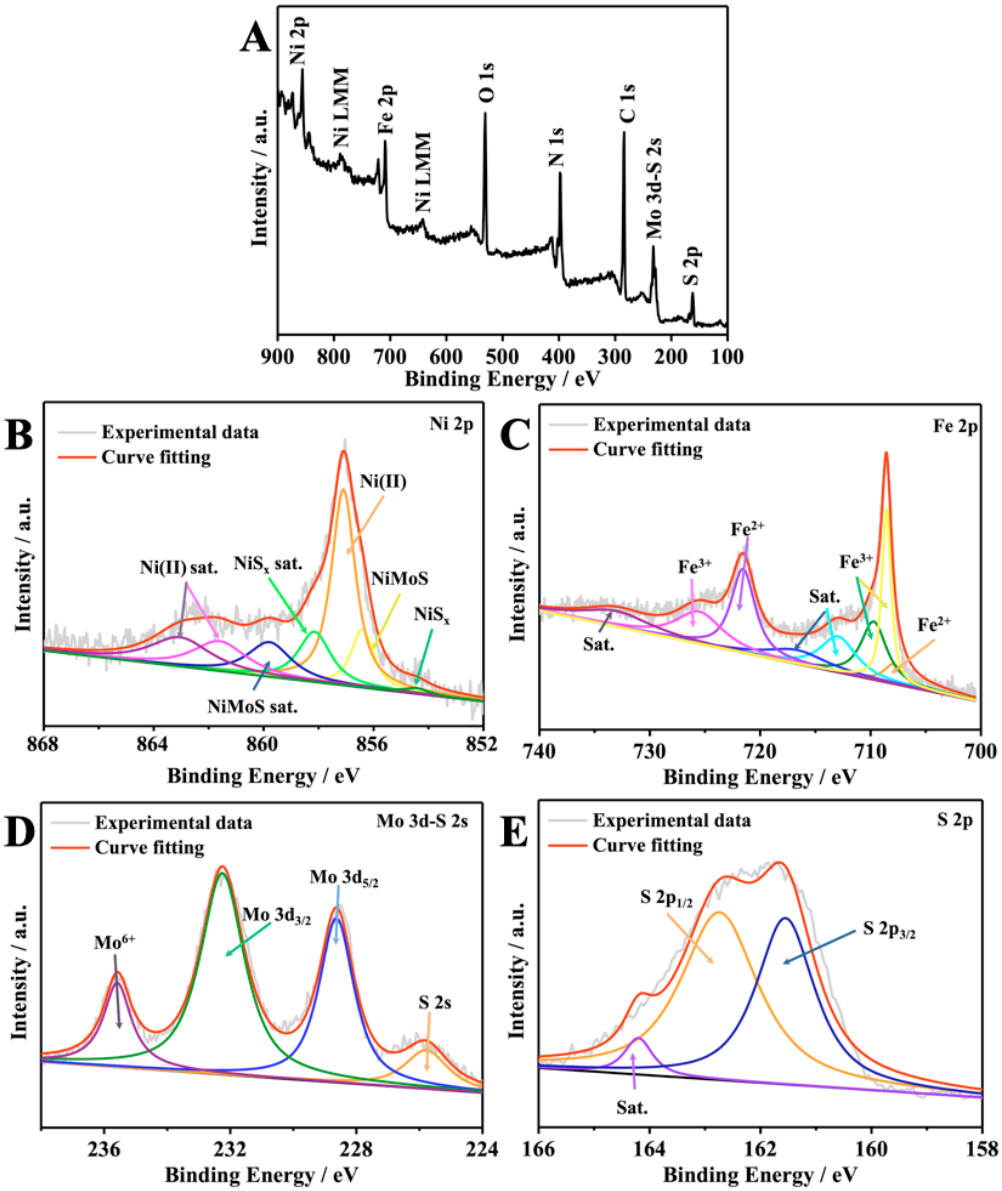


**Figure S16.** (A) XPS survey spectrum of Nanocages after reacting with DA, and (B-E) high-resolution XPS spectra of Ni 2p, Fe 2p, Mo 3d-S 2s and S 2p.

**Table S1.** Comparison of the kinetic parameters of laccase-like activity between Nanocages and natural laccase.

| Material | Substrate | $K_m$ | $V_{max}$ / ($10^{-8}$ M $s^{-1}$) |
|---|---|---|---|
| Nanocages | Dopamine | 9.82 μM | 3.67 |
| Laccase | Dopamine | 18.05 μM | 1.21 |

**REFERENCES**

(S1) Cao, Z. K.; Duan, A. J.; Zhao, Z.; Li, J. M.; Wei, Y. C.; Jiang, G. Y.; Liu, J. A simple two-step method to synthesize the well-ordered mesoporous composite Ti-FDU-12 and its application in the hydrodesulfurization of DBT and 4,6-DMDBT. *J. Mater. Chem. A* **2014**, *2*, 19738-19749.

(S2) Lai, W. K.; Chen, Z.; Zhu, J. P.; Yang, L. F.; Zheng, J. B.; Yi, X. D.; Fang, W. P. A NiMoS flower-like structure with self-assembled nanosheets as high-performance hydrodesulfurization catalysts. *Nanoscale* **2016**, *8*, 3823-3833.

(S3) Ahn, W.; Park, M. G.; Lee, D. U.; Seo, M. H.; Jiang, G. P.; Cano, Z. P.; Hassan, F. M.; Chen, Z. W. Hollow multivoid nanocuboids derived from ternary Ni-Co-Fe Prussian blue analog for dual electrocatalysis of oxygen and hydrogen evolution reactions. *Adv. Funct. Mater.* **2018**, *28*, 1802129.

(S4) Peng, H.; Lu, J.; Wu, C. X.; Yang, Z. X.; Chen, H.; Song, W. J.; Li, P. Q.; Yin, H. Z. Co-doped $MoS_2$ NPs with matched energy band and low overpotential high efficiently convert $CO_2$ to methanol. *Appl. Surf. Sci.* **2015**, *353*, 1003-1012.

(S5) Cao, M. H.; Wu, X. L.; He, X. Y.; Hu, C. W. Shape-controlled synthesis of Prussian blue analogue $Co_3[Co(CN)_6]_2$ nanocrystals. *Chem. Commun*. **2005**, 2241-2243.

(S6) Dai, X. P.; Du, K. L.; Li, Z. Z.; Liu, M. Z.; Ma, Y. D.; Sun, H.; Zhang, X.; Yang, Y. Co-doped $MoS_2$ nanosheets with the dominant CoMoS phase coated on carbon as an excellent electrocatalyst for hydrogen evolution. *ACS Appl. Mater. Interfaces* **2015**, *7*, 27242-27253.

(S7) Li, C. Q.; Zhao, X.; Liu, Y. W.; Wei, W.; Lin, Y. Q. 3D Ni-Co sulfoxide nanosheet arrays electrodeposited on Ni foam: a bifunctional electrocatalyst towards efficient and stable water splitting. *Electrochim. Acta* **2018**, *292*, 347-356.

(S8) Li, Y.; Wen, H. J.; Yang, J.; Zhou, Y. Z.; Cheng, X. N. Boosting oxygen reduction catalysis with N, F, and S tri-doped porous graphene: tertiary n-precursors regulates the constitution of catalytic active sites. *Carbon* **2019**, *142*, 1-12.

(S9) Tang, T.; Jiang, W. J.; Niu, S.; Liu, N.; Luo, H.; Chen, Y. Y.; Jin, S. F.; Gao, F.; Wan, L. J., Hu, J. S. Electronic and morphological dual modulation of cobalt carbonate hydroxides by Mn doping toward highly efficient and stable bifunctional electrocatalysts for overall water splitting. *J. Am. Chem. Soc*. **2017**, *139*, 8320-8328.

(S10) Sun, F. Z.; Li, C. Q.; Li, B.; Lin, Y. Q. Amorphous $MoS_x$ developed on $Co(OH)_2$ nanosheets generating efficient oxygen evolution catalysts. *J. Mater. Chem.*

*A* **2017**, *5*, 23103-23114.

(S11) McCrory, C. C.; Jung, S.; Peters, J. C.; Jaramillo, T. F. Benchmarking heterogeneous electrocatalysts for the oxygen evolution reaction. *J. Am. Chem. Soc.* **2013**, *135*, 16977-16987.

(S12) Wu, H. B.; Xia, B. Y.; Yu, L.; Yu, X. Y.; Lou, X. W. Porous molybdenum carbide nano-octahedrons synthesized via confined carburization in metal-organic frameworks for efficient hydrogen production. *Nat. Commun.* **2015**, *6*, 6512.

(S13) Wang, T.; Liu, L.; Zhu, Z.; Papakonstantinou, P.; Hu, J.; Liu, H.; Li, M. Enhanced electrocatalytic activity for hydrogen evolution reaction from self-assembled monodispersed molybdenum sulfide nanoparticles on an Au electrode. *Energ. Environ. Sci.* **2013**, *6*, 625-633.